Fermilab Library
0 1160 0038834 2

Reprinted from
Proceedings of the [illegible] Conf.
on High-Energy Accelerators and
Instrumentation - [illegible] 1959

MURA [illegible]

COMPARISON OF EXPERIMENTAL RESULTS WITH THE THEORY OF RADIO-FREQUENCY ACCELERATION PROCESSES IN FFAG ACCELERATORS

L. W. Jones (*), C. H. Pruett, K. R. Symon and K. M. Terwilliger (*)

Midwestern Universities Research Association, Madison, Wis. (**)

(presented by K. R. Symon)

I. INTRODUCTION

A theory of radio-frequency acceleration processes in fixed field accelerators was presented at the 1956 CERN Symposium[1]. It is the purpose of this paper to report additional theoretical results and experiments carried out with the MURA 400 keV radial sector electron accelerator[2].

It has been shown[1] that the variable

$$W = \int \frac{dE}{f(E)}, \tag{1}$$

where $f(E)$ is the frequency of revolution at energy E, is canonically conjugate to the phase ϕ of the particle relative to the accelerating voltage. We may see this easily if we note that the equations of motion are, if we replace the f voltage kicks per second by a steady energy gain $f\,V \sin\phi$, (note that V and E are measured in the same units)

$$\frac{dW}{dt} = V(t)\sin\phi\,,$$
$$\frac{d\phi}{dt} = 2\pi h(f_s(t) - f(W))\,, \tag{2}$$

where the peak voltage V and oscillator frequency $h f_s$ are given functions of t, the particle frequency f is known as a function of W from Eq. (1), and h is the harmonic number. (We deviate slightly from Symon and Sessler[1] in that we define ϕ in the more conventional way as the phase of the oscillator when the particle arrives at the accelerating gap, with $\phi = 0$ when the RF voltage is zero and increaisng. In the same notation as in the above[1], our $\phi = \pi - h\Theta^*$.) These equations are derivable from the Hamiltonian

$$H(W, \phi, t) = V(t)\cos\phi + 2\pi h f_s(t) W - 2\pi h E(W)\,. \tag{3}$$

Hence during any acceleration process, the phase points W, ϕ move according to the dynamical equations as an incompressible fluid.

When a frequency modulated accelerating voltage is applied, there is a region of stable phase oscillations (a " bucket ") in which particles may be accelerated in synchronism with the radio-frequency, as shown in Fig. 1. It is convenient, in plotting particle paths, to introduce the variable

$$y = \left[\frac{2\pi h|\kappa_s|}{E_s V}\right]^{\frac{1}{2}} (W - W_s) f_s\,, \tag{4}$$

where the subscript " s " refers to the synchronous particle, and

$$\kappa = \frac{E}{f}\frac{df}{dE} = \frac{1 - \dfrac{\gamma^2}{k+1}}{\gamma^2 - 1} \tag{5}$$

$$\gamma = \frac{E}{mc^2}\,, \qquad k = \frac{R}{\langle B\rangle_{av}}\frac{d\langle B\rangle_{av}}{dR}$$

(*) University of Michigan, Ann Arbor, Mich.

(**) Supported by the United States Atomic Energy Commission

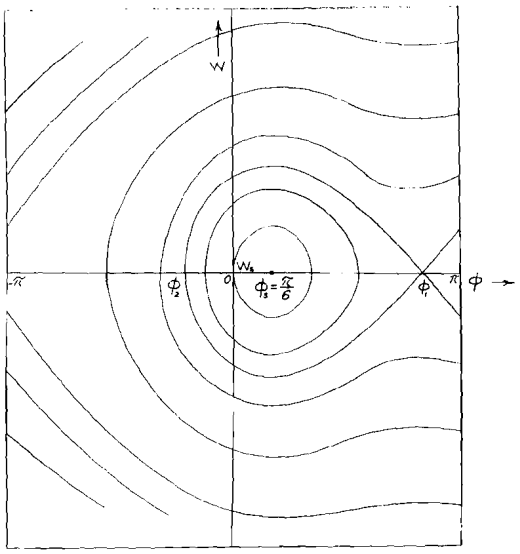

Fig. 1 A frequency modulated bucket. Γ 0.5.

The paths plotted in Fig. 1 are then given by formula (75) of Symon and Sessler [1]:

$$\mp \tfrac{1}{2} y^2 + \cos\phi + \Gamma\phi = C\,, \qquad (6)$$

where the sign applies below the transition energy ($\kappa > 0$), Γ $\sin\phi_s$, and C is constant along a phase curve. Formulas for the area and dimensions of the bucket have been given [1, 3]. Since the phase points move as an incompressible fluid, if n buckets of area A containing N particles each are accelerated to a given energy and stacked, the stacked beam of n N particles must occupy an area at least equal to n A on the W, ϕ phase cylinder. Correspondingly, if a bucket of area A is accelerated past a group of particles outside it, these particles must on the average move downward in energy by an amount

$$\langle \Delta E \rangle_{\mathrm{av}} = f \langle \Delta W \rangle_{\mathrm{av}} = \frac{fA}{2\pi}\,. \qquad (7)$$

These and other theoretical predictions have been checked both by digital computation and by experiment.

The MURA 400 keV radial sector electron accelerator has been described previously [2, 4]. In order to apply a radio-frequency accelerating voltage to the electrons, a fraction of the voltage developed across the resonant circuit of an oscillator is applied directly across an insulating gasket between the two halves of the vacuum chamber, as described in more detail by Terwilliger et al.[3]. The circuit is capable of frequency modulation over a 10 Mc/s range in the 35 to 75 Mc/s region with avariable repetition time down to about 100 μs, and supplies a peak RF voltage of 50 V. A later circuit using a master oscillator and power amplifier, was used in the beam capture experiments. It can supply a larger voltage, with a controllable rise and fall time of the RF voltage. In the experiments, a beam is accelerated to about 300 keV by a betatron pulse, there is then a period of a few milliseconds during which an RF experiment is performed, followed by a final analyzing betatron pulse which sweeps any remaining beam on to a target at 365 keV. X-rays from the target are detected with a photomultiplier whose output is displayed on a cathode-ray trace. An example is shown in Fig. 2, where we see in the top trace the accelerating voltage due to the two betatron pulses with an RF accelerating voltage between, and in the second trace the photomultiplier output showing a part of the beam accelerated onto the target by the RF, and the remainder of the beam arriving during the second betatron pulse. The time scale was 500 μs/cm on the trace. The case with which RF experiments can be performed and analyzed represents a great advantage for an FFAG experimental accelerator.

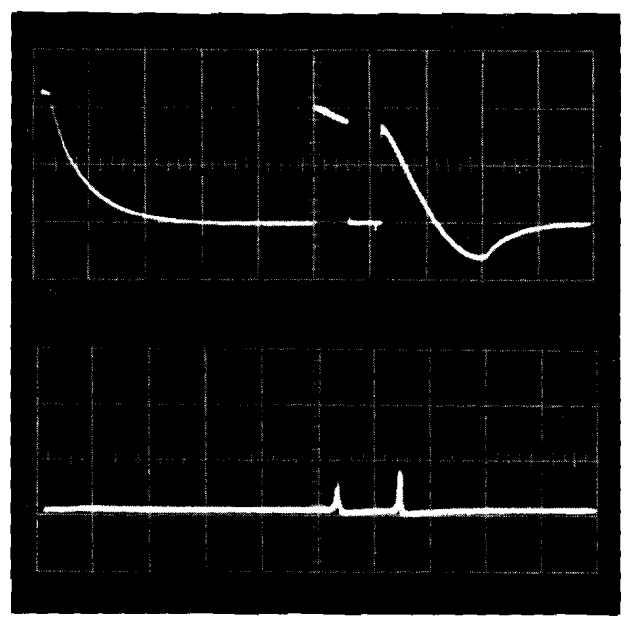

Fig. 2 Oscilloscope trace showing RF acceleration.
Upper trace. Betatron and peak RF accelerating voltage.
Lower trace. Photomultiplier output.

II. PHASE DISPLACEMENT THEORY

In beam stacking accelerators, it is of interest to study the behavior of a coasting beam when a frequency modulated RF bucket is accelerated (or decelerated) past it. As noted above, it is a consequence of Liouville's theorem that on the average, the particles outside the bucket must be displaced in energy by an amount $\langle \Delta E \rangle_{av}$ given by formula (2). There will, however, be a statistical distribution in the displacements ΔE suffered by the individual particles, which is given by formula (85) of Symon and Sessler [1]:

$$\Delta E = \left[\frac{EV}{\pi h|\kappa|}\right]^{\frac{1}{2}} I(\Gamma, \phi_0) , \tag{8}$$

with

$$I(\Gamma,\phi_0) = \int_{\phi_0}^{\infty} \frac{\sin\phi \, d\phi}{[\cos\phi - \cos\phi_0 + \Gamma(\phi - \phi_0)]^{\frac{1}{2}}} , \tag{9}$$

where ϕ_0 is the phase at which the displaced particle becomes synchronous with the RF, (i.e., the phase at $W = W_s$ in Fig. 1). The integral I has been evaluated numerically for various values of Γ, ϕ_0.

A beam initially distributed uniformly in phase and energy over a small energy spread in the W, ϕ-space will not show a uniform distribution in ϕ_0. A particle initially at a point y_1, ϕ_1 far from the bucket ($y_1 \gg 1$) will pass the bucket at phase ϕ_0 given by Eq. (6) (we choose the upper sign for convenience),

$$\cos\phi_0 + \Gamma\phi_0 = -\tfrac{1}{2}y_1^2 + \cos\phi_1 + \Gamma\phi_1 . \tag{10}$$

Particles at a given ϕ_1 with an energy spread given by dy_1 will pass the bucket at a value of ϕ_0 within a range $d\phi_0$ given by

$$dy_1 = -\frac{\Gamma - \sin\phi_0}{y_1} d\phi_0 . \tag{11}$$

Since y_1 is uniformly distributed, ϕ_0 will have the (normalized) probability distribution

$$P(\phi_0)d\phi_0 = \frac{\Gamma - \sin\phi_0}{2\pi\Gamma} d\phi_0 . \tag{12}$$

Note that there is a range of values of ϕ_0 ($\phi_1 < \phi_0 < \phi_2$ in Fig. 1) which is inaccessible to particles initially outside the bucket. We define a variable

$$q = \int_{-\pi}^{\phi_0} \frac{\Gamma - \sin\phi}{2\pi\Gamma} d\phi , \tag{13}$$

running from 0 to 1 as ϕ_0 runs from $-\pi$ to π. (The range $\phi_1 < \phi_0 < \phi_2$ is to be excluded from the integral (13).) We have then

$$P(q)dq = P(\phi_0)d\phi_0 = dq , \tag{14}$$

so that q is uniformly distributed. A graph of q vs. ϕ_0 is shown in Fig. 3. We may note in passing that the path given by Eq. (6) for large y oscillates about a helix on the W, ϕ-cylinder of pitch

$$\Delta y = \frac{2\pi\Gamma}{y} . \tag{15}$$

Since particles with different ϕ_0 suffer different displacements, in order to get a proper statistical sample of orbits starting from a large initial y_1, it is necessary to take a uniform distribution of particles throughout an energy spread equal to one or more times the pitch given by formula (15), a point which must be kept in mind in planning computer studies of RF processes.

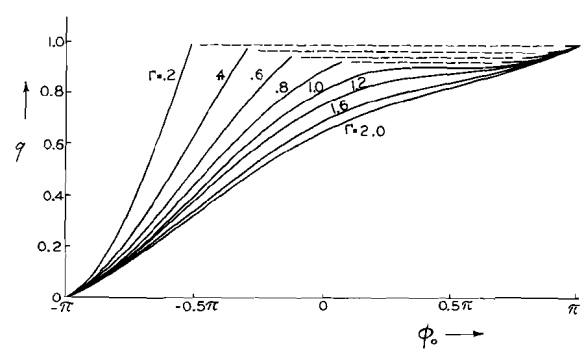

Fig. 3 Plot of $q = \frac{\varphi_0 + \pi}{2\pi} + \frac{\cos\varphi_0 + 1}{2\pi\Gamma}$.

The integral I is plotted as a function of q for several values of Γ in Fig. 4. Since equal intervals of q are equally likely, we can see that the distribution in energy of an initially monoenergetic beam will,

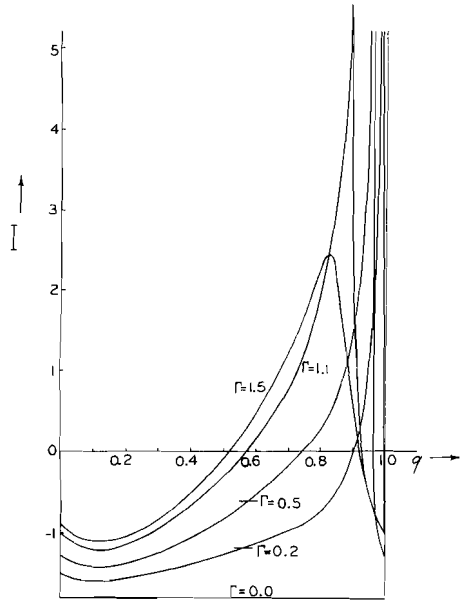

Fig. 4 Phase displacement integral $I(\Gamma, q)$.

after phase displacement downward, be as shown in curve (a) of Fig. 5. There is a sharply defined minimum energy peak, and a tail stretching out to higher energies, ending in a thin umbilicus which in principle reaches to the final bucket position. It can be shown that the number of particles in the umbilicus falls off exponentially with energy as

$$P(E)dE \propto \exp\left[-\frac{(1-\Gamma^2)^{\frac{1}{4}}}{\sqrt{2}\Gamma} I\right]. \qquad (16)$$

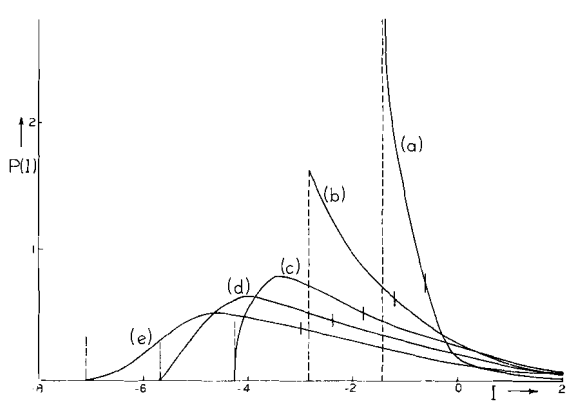

Fig. 5 Energy distribution after (*a*) one, (*b*) two, (*c*) three, (*d*) four, (*e*) five displacements of a monoenergetic beam. Single dashes indicate mean displacements. Dashed lines indicate maximum displacements.

The mean value of I, given by Eqs. (7) and (8), is indicated by a dash on the curves in Figs. 4 and 5. By folding the distribution $P(I)$ into itself, we obtain the (approximate) curves (b), (c), (d), (e) in Fig. 5, which show the beam distribution after two, three, four and five successive displacements. When the initial beam is not monoenergetic, its initial distribution must also be folded in. Fig. 5 is drawn for $\Gamma = 0.5$. For smaller values of Γ, the maximum displacements are closer to the mean displacement. We give in Table 1 the mean $\langle I \rangle_{av}$ and maximum displacement I_{max} for several values of Γ.

TABLE I

Γ	$\langle I \rangle_{av}$	I_{max}
1.7	0	− 1.06
1.3	0	− 1.14
0.9	− 0.073	− 1.27
0.5	− 0.60	− 1.42
0.3	− 0.97	− 1.54
0.1	− 1.44	− 1.68
0.0	− 1.80	− 1.80

III. BEAM STACKING EXPERIMENTS

Experiments designed to test the theory of beam stacking have been reported elsewhere [3]; the results will be reviewed briefly here. Preliminary measurements were made of threshold RF voltage for acceleration, of the energy spread of the beam at 300 keV, and of the energy spread ΔE of the RF bucket. These measurements are made by switching on the oscillator voltage suddenly during the FM cycle when the frequency is synchronous with the beam revolution frequency or is slightly above or below it, and noting whether any beam is captured and accelerated. The results are in agreement with theory within the experimental error (about 10 per cent). The theoretical calculation of threshold voltage and bucket size requires a knowledge of the parameter df/dE, which can be calculated from formula (5) when f, E and k are known, or better, measured by varying the beam energy around 300 keV and measuring the change in RF capture frequency. Interestingly enough, the most accurate experimental measurement of electron energy is obtained by measuring df/dE and calculating E from formula (5).

Fig. 6 shows a record of a phase displacement experiment. The RF frequency modulation in this case is not sufficient to accelerate from 300 keV to the target, and so no beam appears on target until the analyzing betatron pulse, which is shown in the top trace on an expanded time scale (20 μs/cm). The vertical scale in the top trace is 5 V/cm. In the remaining traces we see the beam arriving on target during the analyzing betatron pulse. In each case, two complete RF modulation cycles were carried out before the analyzing betatron pulse. In the second trace, the RF is turned on when the frequency is above the beam revolution frequency and the result is the same as if the RF is not turned on at all. The time between the beginning of the second betatron pulse and the beam pulse represents the time required to accelerate the beam on to the target and is therefore proportional to the energy difference between the original coasting beam and the target. In the third trace, the turn-on frequency is synchronous with the beam, and most of the beam is captured and accelerated. In the fourth trace, the RF turn-on frequency is below the revolution frequency of the original coasting beam. No beam is captured, and instead the beam is phase – displaced downward in energy, hence arrives at the target about 24 μs later than in the second trace. From the betatron voltage (7 V/turn) and the revolution frequency (73.5 Mc/s), the amount of phase displacement can be calculated (12.4 keV). This is then the phase displacement for two RF modulation cycles. Up to seven or eight successive RF modulation cycles can be applied before the second analyzing pulse, and the measured phase displacement is proportional to the number of modulation cycles. In Table II we compare the measured average displacement per cycle (i.e., the displacement of the top of the beam pulse) after two modulation cycles with the theoretical values calculated from formula (7), for two voltages, hence two values of Γ. It is clear from Fig. 5 that the interpretation of the top of the beam pulse as the average is open to question, unless the initial beam energy spread is larger than the phase displacement; in this case, it is somewhat larger. The theoretical maximum displacement is compared in Table II with the measured displacement of the right-hand edge of the beam pulse (32 μs between the second and fourth traces in Fig. 6). The results are within experimental error, and suggest a systematic error of the order of 20 per cent. An alternative method of measuring the phase displacement in say two cycles, is to adjust the RF turn-on frequency so that the beam is accelerated on the third cycle. The difference between this frequency and the beam revolution frequency is a measure of the displacement. In this case it is difficult to say precisely what is measured when the RF turn-on frequency is tuned for maximum beam on the third cycle. The measured displacement lies between the theoretical maximum and average values as would be predicted from the theoretical statistical distribution of the displaced beam.

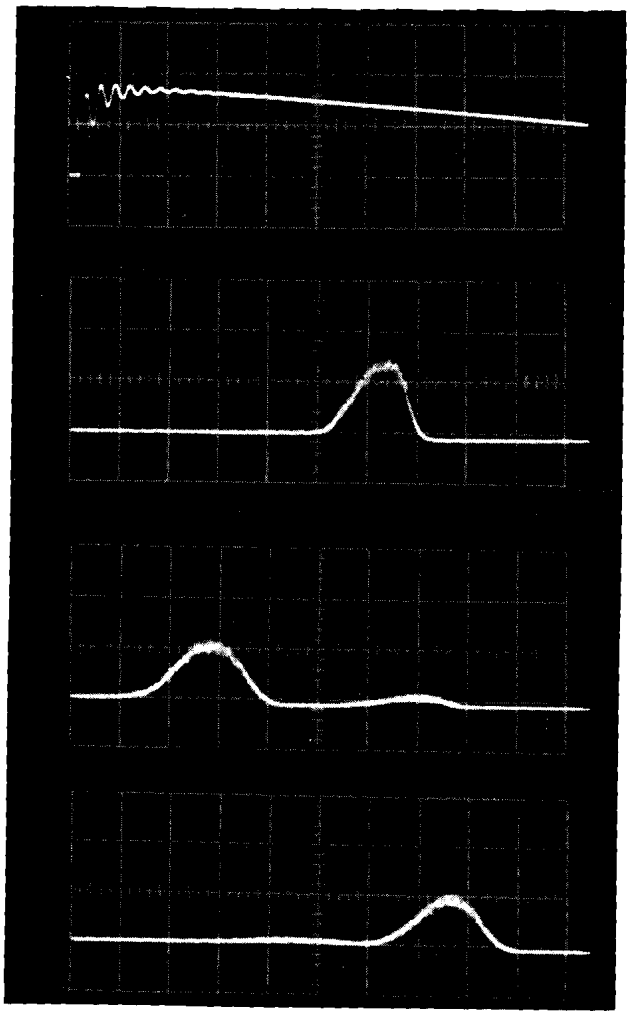

Fig. 6 Phase displacement.
First trace: Second betatron pulse.
Second trace: Photomultiplier output. RF turn-on above beam frequency.
Third trace: RF turn-on at beam frequency.
Fourth trace: RF turn-on below beam frequency.

TABLE II

Phase displacement measured with two RF modulation cycles

RF Voltage Peak	Γ		Energy loss per RF cycle Average	Maximum	Ratio max/ave
42.5	0.196	measured	6.2	7.6	1.23
		calculated	7.4	9.9	1.35
28	0.30	measured	3.8	5.7	1.50
		calculated	4.9	7.8	1.59

A simulated beam stacking experiment is shown in Fig. 7. The experiment is similar to the phase displacement experiment described above, except that the second betatron pulse is delayed 5 ms to permit up to 10 RF modulation cycles between betatron pulses. The resulting beam pulses during the second betatron pulse are shown in the five traces in Fig. 7 which correspond respectively to no RF, one, four, seven and ten RF modulation cycles. Since no beam is added to that initially present, what we see is the history of a single injected beam pulse after from one to ten RF modulation cycles. The first cycle carries most of the beam to the " stacking " energy (340 keV). The next three cycles displace it about 2/5 of the way down to the " injection " energy (300 keV), at the same time accelerating most of the remaining beam to 340 keV. After seven pulses, the initial pulse has been displaced nearly back to 300 keV. After ten pulses, the beam has been accelerated a second time. The energy scattering due to the statistical distribution of the phase displacement energy is clearly visible. In an actual stacking process a new beam pulse would be injected before each modulation cycle, and hence the traces of Fig. 7 after one, two, three and four modulation cycles should be added to find the stacked beam after say four cycles.

IV. RF KNOCKOUT

If radio-frequency electric fields act on the particles in an accelerator, then RF knockout resonances may occur which make the betatron oscillations unstable if the relation [2]

$$p\nu_x + q\nu_y = \pm m \pm f_{rf}/f\,, \qquad (17)$$

is satisfied, where f_{rf} is the radio-frequency, f is the revolution frequency of the beam, m, p, q are positive integers ($p+q \leq 4$), and ν_x, ν_y are numbers of radial and vertical betatron oscillations per revolution. This effect has been utilized to measure ν_x and ν_y [2]. It is clear that for particles in an RF bucket ($f_{rf} = h f$) relation (17) cannot be satisfied unless ν_x, ν_y already lie on a resonance for betatron oscillations alone. In beam stacking machines, however, it is important to insure that the stacked beam is not subject to RF

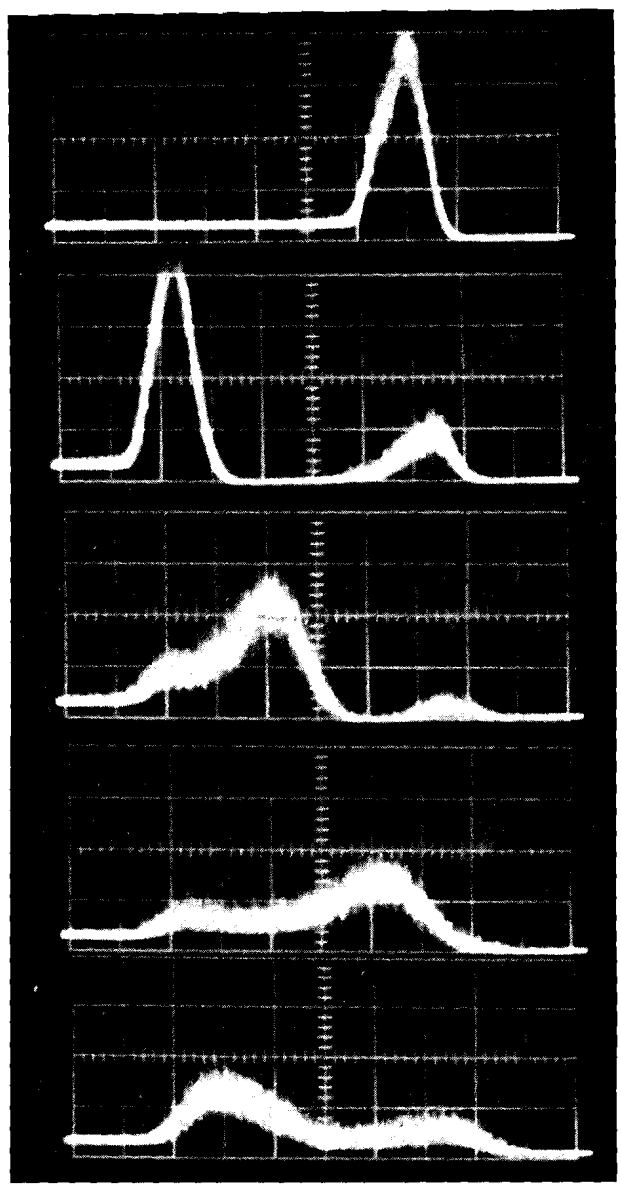

Fig. 7 A beam stacking experiment. Traces show photomulitplier output after zero, one, four, seven, and ten successive modulation cycles.

knockout by the accelerating voltages which bring up new particles.

Integral knockout resonances ($p+q=1$) are by far the most serious and are indeed the only ones which have been detected in RF acceleration experiments. Radial resonances ($p=1$, $q=0$) are driven by RF field components exerting forces either radially or azimuthally. Vertical resonances ($p=0$, $q=1$) are driven by vertical force components, which should be very small in an accelerating gap with median plane symmetry. Half integral resonances ($p+q=2$) are driven by gradients in the RF fields and have been observed with RF knockout probes specifically designed for that purpose [2]. Non-linear knockout resonances ($p+q>2$) are driven by non-linear RF fields and have not as yet been observed.

The integer m in Eq. (17) represents the harmonic order of the azimuthal distribution ($\sin m\theta$ or $\cos m\theta$) of the RF voltage which drives the resonance. For a single accelerating gap at $\theta=0$, the azimuthal distribution is essentially $\delta(\theta)$, so that all values of m (up to $2\pi R/g$, where g is the accelerating gap width) are equally dangerous. By appropriate spacing and phasing of accelerating gaps, it is possible to eliminate certain azimuthal harmonics m from the RF voltage and hence eliminate certain RF knockout resonances. If we consider, for example, a stacked beam with revolution frequency f_1, and an RF accelerating voltage bringing up beam on the hth harmonic, then a radial integral resonance occurs if

$$f_s = \left|\frac{\nu_x \pm m}{h}\right| f_1 \,. \tag{18}$$

At the stack point $f_s = f_1$, relation (18) cannot be satisfied unless ν_x is an integer. If we are below the transition energy, the nearest resonance occurs when m is chosen so that $\left|\frac{\nu_x \pm m}{h}\right|$ is a fraction closest to unity. For $h=1$, the largest fraction $|\nu_x \pm m|$ will be of order $\frac{1}{2}$ to $\frac{3}{4}$, and this sets a limit on the allowed range of frequency modulation if no knockout resonance is to be crossed. For $h>1$, the range is even more limited. Over a wide range of frequency modulation, Δf_s, there are roughly $h\Delta f_s/f_1$ knockout resonances. If h equally spaced accelerating gaps are used in phase with equal voltages, then (except for voltage and phase errors) only those resonances where m is a multiple of h appear. With $2h$ gaps alternately phased, only odd multiples of h lead to resonances.

We now calculate the build-up of betatron amplitudes when f_{rf} is modulated through an integral resonance. Let x, p be the coordinate and a suitable momentum so scaled that the phase curves in x, p-space are circles. We define a complex vector Z by

$$x+ip = Ze^{-2\pi i \int \nu f dt} \,. \tag{19}$$

The vector Z represents the amplitude and phase of betatron oscillations in a coordinate system rotating with the betatron oscillations in the x, p-plane, so that in the absence of external forces, Z is constant. When the particle crosses an RF accelerating gap $t=t_i$, it receives increments in x and p proportional to the gap voltage, which we shall calculate below. Let Δx_0, Δp_0 be the increments at peak cavity voltage, and set

$$\Delta x_0 = a\cos\delta \,, \quad \Delta p_0 = a\sin\delta \,. \tag{20}$$

Then at time t_i,

$$\Delta(x+ip)_i = ae^{i\delta}\cos\left(\int_0^{t_i} 2\pi i \nu f_{rf} dt + \lambda\right) . \tag{21}$$

Since the times t_i differ by complete periods of revolution, we can without changing the value of $\Delta(x+ip)_i$, add a term $\pm mf$ to the integrand in Eq. (21). Hence,

$$(\Delta Z)_i = \tfrac{1}{2} ae^{i(\delta+\lambda)} e^{2\pi i \int_0^{t_i} (\nu f \pm mf + f_{rf}) dt} + \\ + \tfrac{1}{2} ae^{i(\delta-\lambda)} e^{2\pi i \int_0^{t_i} (\nu f \pm mf - f_{rf}) dt} \,. \tag{22}$$

If we pass through an integral resonance given by formula (17), one or the other of the integrands in Eq. (22) will vanish. We assume that near the resonance the integrand changes at a constant rate $\dot{f}$. ($\dot{f} = \pm \dot{f}_{rf}$ for a stacked beam in an FFAG accelerator; the derivation however applies also if f or ν are changing with time.) We take $t=0$ at resonance, and neglect the non-resonant term:

$$(\Delta Z)_i = \tfrac{1}{2} ae^{i\delta'} e^{\pi i \dot{f} t^2} \,, \quad (\delta' = \delta \pm \lambda) \,. \tag{23}$$

If initially $Z=0$, then after crossing the resonance,

$$Z = \tfrac{1}{2} ae^{i\delta'} \sum_i e^{\pi i \dot{f} t^2} \,. \tag{24}$$

If $\dot{f}^{1/2}/f \ll 1$, the sum may be approximated by an integral:

$$Z = \tfrac{1}{2} a e^{i\delta'} \int_{-\infty}^{\infty} f e^{\pi i \dot{f} t^2} dt$$

$$= \tfrac{1}{2} a f (\pi \dot{f})^{-1/2} e^{i\delta'} \int_{-\infty}^{\infty} e^{iu^2} du$$

$$= \tfrac{1}{2} a f \dot{f}^{-1/2} e^{i(\delta' + \pi/4)}, \tag{25}$$

and

$$|Z| = \tfrac{1}{2} a f / |\dot{f}|^{\frac{1}{2}}. \tag{26}$$

The final amplitude is equivalent to $\frac{1}{2} f/|\dot{f}|^{1/2}$ in phase increments of amplitude a. Since the phase of the RF will be random relative to the phase of betatron oscillations due to other sources or to previous passages through resonance, the amplitude (26) is to be added in quadrature to any amplitude already present to obtain the r.m.s. amplitude after crossing the resonance. In particular, if a given resonance occurs in a stacking process, then after n modulation cycles, the build-up due to this resonance, for the first particles stacked, is $n^{1/2}$ times the value (26).

A particle passing perpendicular to an accelerating gap of voltage V receives an energy increment $\Delta E = V$. With the momentum compaction factor defined by

$$1 + k = \frac{R}{p} \frac{dp}{dR}, \tag{27}$$

where R is the mean radius of the equilibrium orbit,

$$\Delta R = \frac{RV}{(1+k)\beta^2 E}, \quad \left(\beta = \frac{v}{c}\right), \tag{28}$$

and since the radial position of the particle does not change if the gap is narrow, the radial betatron oscillation changes by

$$\Delta x_0 = -\frac{VR}{(1+k)\beta^2 E} = -a, \quad (\delta = \pi). \tag{29}$$

If the particle crosses the gap at an angle η to the normal, it is easy to show that the particle suffers change in direction of amount

$$\Delta\psi = -\frac{V \tan \eta}{\beta^2 E}, \tag{30}$$

and hence an additional amplitude change

$$\Delta p_0 = a_\eta = -\frac{\beta_x R V \tan \eta}{\beta^2 E}, \tag{31}$$

in quadrature with the amplitude change (29). Here $\beta_x R$ is the matrix parameter relating position and angle for one revolution:

$$\begin{pmatrix} x \\ \psi \end{pmatrix}_1 = \begin{pmatrix} (\cos 2\pi\nu_x + \alpha_x \sin 2\pi\nu_x) & \beta_x R \sin 2\pi\nu_x \\ \dfrac{1+\alpha_x^2}{\beta_x R} \sin 2\pi\nu_x & (\cos 2\pi\nu_x - \alpha_x \sin 2\pi\nu_x) \end{pmatrix} \begin{pmatrix} x \\ \psi \end{pmatrix}_0. \tag{32}$$

For sinusoidal oscillations,

$$\beta_x = \frac{1}{\nu_x}, \tag{33}$$

and for most alternating gradient accelerators,

$$\beta_x \simeq \frac{2}{\nu_x}. \tag{34}$$

Hence finally,

$$a = \frac{VR}{\beta^2 E(1+k)} [1 + (1+k)^2 \beta_x^2 \tan^2 \eta]^{\frac{1}{2}}, \tag{35}$$

$$\tan \delta = \frac{-\beta_x \tan \eta}{-(1+k)}. \tag{36}$$

In typical cases, the increase in betatron amplitude due to integral knockout resonances turns out to be important in a beam stacking accelerator, but often tolerable if η is small, and if only a few resonances are crossed per modulation cycle. In the MURA 40 MeV two-way electron accelerator, for example, there is a knockout resonance which lies just below the pick-up energy for the RF modulation cycle. If the parameters were altered slightly, so that this resonance were crossed, the resultant build-up in betatron amplitude could be 0.5 cm after 100 modulation cycles. With 100 cycles per second, this is about comparable to the build-up due to gas scattering at 10^{-6} mm Hg.

Experiments on knockout by RF accelerating voltages in the MURA 400 keV radial sector accelerator have been carried out using the RF system described above. First, the RF knockout frequencies at the target radius were determined with the RF probes designed for that purpose [2]. Table III lists the knockout frequencies thus found and the resultant ν values.

TABLE III

f_{rf} (Mc/s)	Character	
12.1	vertical, $\nu_y = 2 - f_{rf}/f$	$f = 12.1 + 61.2 = 73.3$
15.4	radial, $\nu_x = 3 - f_{rf}/f$	$f = 15.4 + 58.3 = 73.7$
58.3	radial, $\nu_x = 2 + f_{rf}/f$	$\langle f \rangle_{av} = \frac{73.3 + 73.7}{2} = 73.5$
61.2	vertical, $\nu_y = 1 + f_{rf}/f$	$\nu_x = \frac{58.3}{73.5} + 2 = 2.79$
		$\nu_y = \frac{61.2}{73.5} + 1 = 1.83$

The beam was then allowed to coast for two milliseconds at an energy of 300 keV corresponding to a circulating frequency, f, of about 72.2 Mc/s. During this coasting period, the frequency modulated RF oscillator was pulsed on for a short time. This oscillator, tied across the accelerating gap as for RF acceleration, was tuned to sweep the range 55-61 Mc/s. Effects on the coasting beam were clearly apparent when the frequency crossed 55.9 Mc/s (radial knockout) and 60.0 Mc/s (vertical knockout).

When the RF was turned on at about 58 Mc/s and the turn-off frequency, f_T, varied, it was found that the beam subsequently accelerated by the second betatron pulse was attenuated partly when f_T was 59.8 Mc/s and was completely destroyed when it was extended to 60.2 Mc/s. With the gap voltage reduced to about 5 V and a rate-of-frequency modulation of about 3 kc/s μs the beam was reduced to half intensity by sweeping the RF to a frequency well above 60 Mc/s. The attenuated beam still appeared at the same time on the second betatron pulse and with the same spread and shape, indicating no observable change in the energy or radial oscillation amplitudes of the surviving beam due to the vertical knockout. There should be no vertical knockout if the fields are perfectly symmetric about the median plane. However, in this accelerator the RF is applied to the top of the gap, which has dimensions not negligible compared to a wavelength. The 2 mm gap is about ten inches long so that it is unlikely that this symmetry condition is met, and vertical RF fields might well exist on the median plane. Since it has not been possible to determine these vertical effects quantitatively, calculations were only made from the radial experiments.

With the RF turn-on frequency at 55 Mc/s, f_T was varied around 56 Mc/s. The beam was not destroyed completely by the RF but it was attenuated by as much as a factor of three, and the character of beam as observed during the second betatron pulse was altered. The beam shape as detected by the photomultiplier for successively higher values of f_T is illustrated schematically in Fig. 8. Since it has been found that the energy spread of the beam is quite small, the time spread of the beam has been interpreted as due to the range of radial betatron oscillations; the earlier particles have the largest amplitudes and the later particles the smallest amplitudes. It is also known that ν_x decreases with increasing amplitude. The interpretation of the observed effect then is that at a low f_T only the large amplitude particles are affected, and as f_T is increased, successively smaller amplitudes of oscillation are affected. From the failure of the front edge to move earlier and the attenuation of the beam, there appears to be a limiting radial amplitude. The range of f_T represented by the extreme cases of Fig. 8 is less than 400 kc/s, corresponding to a range of ν_x, values less than 0.007.

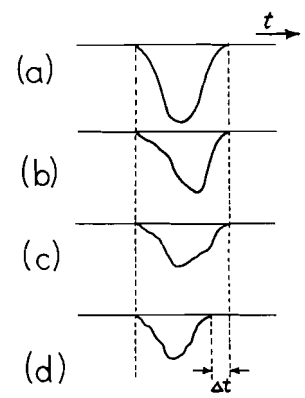

Fig. 8 Beam pulse after RF knockout.
(*a*) Low RF turn-off frequency. Beam unaffected.
(*b*) Higher turn-off frequency. Leading edge of beam affected.
(*c*) Still higher turn-off frequency. Center of beam affected.
(*d*) Highest turn-off frequency. Trailing edge of beam affected.

A quantity which can be determined is the time shift, Δt, of the tail of the pulse, corresponding to the amplitude increase of the smallest amplitude particles, Table IV lists measurements of Δt for different RF conditions and the corresponding radial amplitude increase Δx, which then can be calculated from the betatron voltage, revolution frequency, and from dE/dr.

TABLE IV

V_{rf}	$\frac{df_{rf}}{dt}$	Δt (crude estimate)	Δx	Δx calc.	$\frac{\Delta x \text{ calc.}}{\Delta x \text{ obs.}}$
24 V	9.3×10^9 c/s²	15 μs	1.4 mm	2.4 mm	1.7 mm
14.5	8.0×10^9	11	1.0	1.6	1.6
7.5	3.8×10^9	7.5	0.7	1.3	1.9

These Δx determinations are quite crude (to a factor of two or so) since they involve interpreting a time shift and a shape change as some equivalent Δx. We show also the values of Δx calculated from formulas (26) and (35). (The value of a for 24 V RF is 6×10^{-3} mm. The corresponding value of $\frac{1}{2}f/\dot{f}^{1/2}$ is 400.) The discrepancy is not unreasonable, and many even be due in part to non-linear detuning effects which limit the observed amplitudes.

V. CAPTURE OF PARTICLES INTO A STATIONARY BUCKET

If the radio-frequency is constant, the particles move on the phase curves given by Eq. (6) with $\Gamma = 0$, as shown in Fig. 9. If the voltage V is suddenly turned on from zero to its final value, any particle initially present will move along the phase curve on which it finds itself at the instant of turn-on. A monoenergetic group of particles initially on a line y in Fig. 9 will, after the voltage is suddenly turned on, be distributed among the various phase curves in a manner which is predictable from Fig. 9. It is shown[1] that if the voltage V is turned on sufficiently slowly, then in consequence of the adiabatic theorem a particle which when $V = 0$ lies at a distance ΔE from the synchronous energy, will after V reaches its final value oscillate along a curve of area

$$A = 4\pi\Delta W = 4\pi\Delta E/f, \tag{37}$$

provided of course that this area is less than the total area of the bucket. If it is larger, the particle will move outside the separatrix on a curve such that the area between it and the $y = 0$ axis is $2\pi\Delta W$. It is our present purpose to study deviations from the predicted adiabatic behavior when the voltage is turned on at various finite rates.

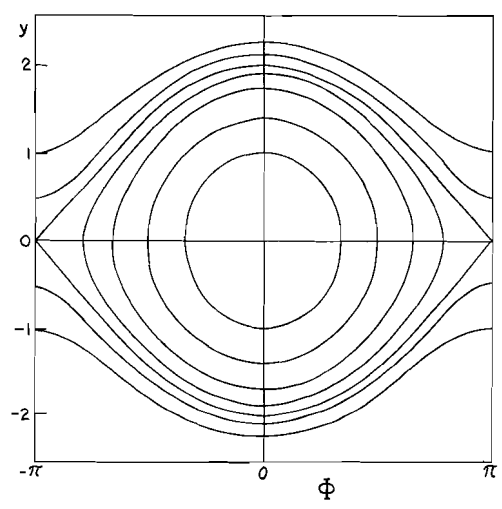

Fig. 9 Stationary bucket (below transition).

The capture process was first investigated by digital computation using a program which calculates $E(t)$, $\phi(t)$ for a particle with given revolution frequency $f(E)$, which receives an energy increment $V(t)\sin\phi$ each time it crosses an accelerating gap. The computations are such that when energies are expressed in terms of the variable y (Eq. (4)), areas of phase curves are expressed in terms of the final bucket area A_s ($A_s = 16$ in y,ϕ units), and times are in units of the final phase oscillation period τ_ϕ, the results are independent of the parameters of the accelerator.

It was first observed that for turn-on times $\tau > \frac{1}{2}\tau_\phi$, all particles within $y_0 < y_a$ given by formula (37) with $A = A_s$ are captured, and no others:

$$y_a = \frac{A_s}{4\pi} = \frac{4}{\pi}. \tag{38}$$

This is the adiabatic result. With $\tau \ll \frac{1}{2}\tau_\phi$ (sudden case), some particles are lost at all values of y, and some particles are captured out to $y_s = \pm 2$ as is to be expected from Fig. 9.

In the limit of adiabatic voltage variation, the initial phase of a particle should be irrelevant to the curve upon which it finally oscillates. Only the initial ΔW should determine the size of the ellipse. Figs. 10 and 11 illustrate the final distribution of captured particles which were initially uniformly distributed in phase and monoenergetic with $y_0 = 0$ and 1. The voltage was turned on linearly from zero to its final value in a time τ. Also listed is the r.m.s. deviation of A/A_s from the value corresponding to a perfectly adiabatic voltage turn-on (Eq. (37)). A broken arrow labeled " ∞ " indicates the adiabatic value of A/A_s. The solid curve labeled " 0 " indicates the

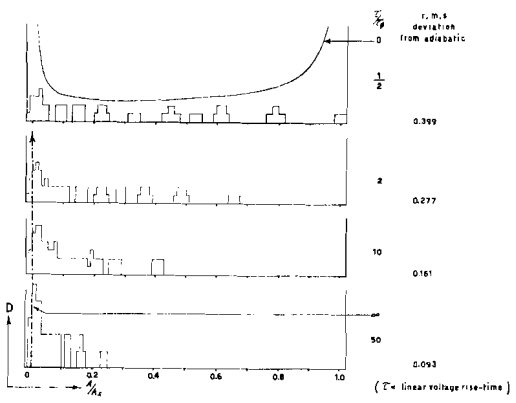

Fig. 10 Distribution of captured particles with linear voltage turn-on ($y_0 = 0$).

theoretical distribution of particles picked up by an instantaneous turn-on. The results confirm what is to be expected from the analytic theory given by Symon and Sessler [1].

Similar computations have been carried out [5] using a non-linear voltage turn-on designed to insure a constant degree of adiabaticity during the turn-on, that is so that the fractional increase in bucket area dA/A in a time dt is proportional to dt/τ_ϕ, where τ_ϕ is the instantaneous period of phase oscillations. The results show that if

$$\frac{dA}{A} = \alpha \frac{dt}{\tau_\phi}, \tag{39}$$

where $\alpha \leq 1$, then the final A/A_s is within about 12 per cent or less of the adiabatic value. Recent calculations by R. Stump [6], including the effect of beam-induced voltages in the cavity, indicate that such effects may be very serious. In the case of the MURA 40 MeV two-way electron accelerator, induced cavity voltages are such as to make a linear voltage turn-on as good as or better than one following the law (39), and to increase considerably the deviation from adiabatic behavior. Presumably longitudinal space charge forces will have a similar effect [7].

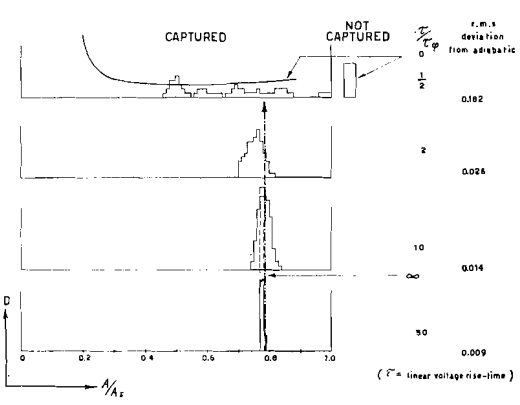

Fig. 11 Distribution of captured particles with linear voltage turn-on. ($y_0 = 1$).

Experiments on the RF capture process have been carried out in the 400 keV radial sector model. A beam is betatron accelerated to 250 keV. A fixed frequency voltage is turned on, at a rate which can be varied, so that the beam is captured. The resultant distribution in amplitude of the phase oscillations is then analyzed by turning the voltage off very slowly, i.e., adiabatically. The above analysis, applied in reverse, shows that beam particles oscillating on a curve of area A will after turn-off be found half at an energy above the synchronous energy by an amount given by formula (37), and half below the synchronous energy an equal amount. The resulting distribution in energy can be analyzed by driving it on to a target by a second betatron pulse as in the studies of phase displacement, or, more accurately, by picking it up by a frequency modulated probing bucket of very small area whose turn-on frequency is precisely controllable.

We show in Fig. 12 an oscillogram of a typical waveform of the RF voltage amplitude. The maximum peak amplitude is 126 V, and the radio frequency is 71.62 Mc/s, and is independent of amplitude. The turn-on time in Fig. 12 is 7 μs, longer than the phase oscillation period, which is 4.1 μs at this energy at $V = 126$ V. The result of a typical experiment with a slow turn-on is shown in Fig. 13, which shows the beam pulse on target during the second betatron pulse. In the top trace, we see the standard beam pulse when no RF is applied. In the second trace, the RF is turned on as in Fig. 12, with the radio-frequency synchronous with the beam. There is no visible effect on the beam, showing that the process is adiabatic. In the third trace, the RF program is identical, but the injection time into the first betatron pulse is slightly later, so that the beam is accelerated to an energy slightly below the synchronous energy. We now see two output pulses, equally spaced above and below the synchronous

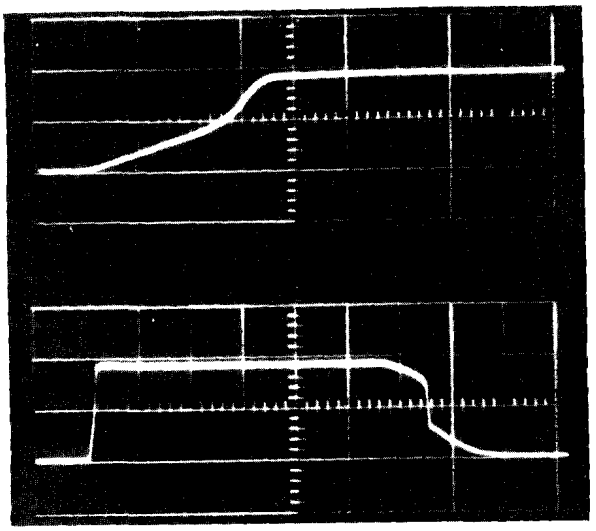

Fig. 12 Amplitude waveform of RF voltage in beam capture experiment.
Lower trace: Complete waveform (50μs/cm).
Upper trace: Expanded turn-on waveform (2μs/cm).

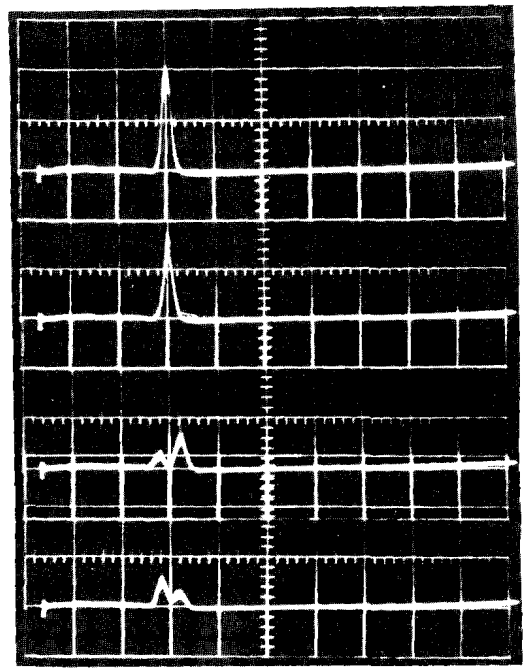

Fig. 13 A beam capture experiment, analyzed by second betatron pulse. Adiabatic turn-on.

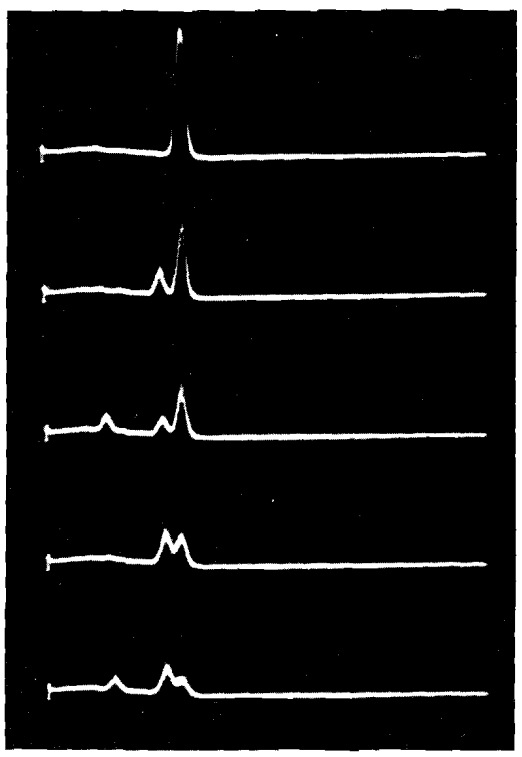

Fig. 14 A beam capture experiment, analyzed by an RF probing bucket. Adiabatic turn-on.

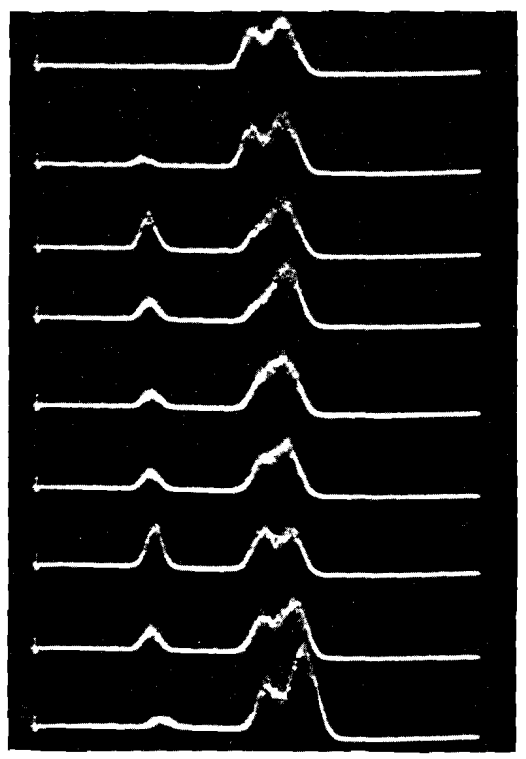

Fig. 15 A beam capture experiment, analyzed by an RF probing bucket. Rapid turn-on.

energy, with no beam at the synchronous energy, in accordance with the theoretical prediction above for an adiabatic turn-on. The fact that the lower energy (later) pulse is larger shows that the beam straddles the edge of the adiabatic capture region (near-y_a in formula (38)), so that only part of the beam is captured. The fourth trace in Fig. 13 shows the corresponding case with the beam initially above the synchronous energy. Fig. 14 shows a similar experiment in which the energy distribution after voltage turn-off is analyzed by means of a frequency modulated probing bucket which is turned on in the beam and modulated to a slightly higher energy. In the first trace, we see the beam when no RF is applied. In the second trace, the capturing RF voltage is turned on and off at a frequency slightly above the beam frequency; this corresponds to trace three of Fig. 13. In the remaining three traces, the capturing RF program is identical, but the probing bucket is turned on after the capturing RF voltage has been turned off. In the third trace, the probing bucket is turned on slightly above the capturing radio-frequency, and we see the sample beam pulse which has been accelerated out of the upper beam pulse. In the fourth trace, the probing bucket is turned on in synchronism with the capturing RF, and we see that there is no beam picked up by the probing bucket, showing that there was no beam at the center of the capturing bucket after turn-on. In the third trace, the probe starts below the synchronous energy. Fig. 15 is a similar record of a capture experiment with rapid turn-on of the capturing RF, at a frequency slightly above the beam frequency. In the top trace, we see the beam as analyzed by the second betatron pulse. In the remaining eight traces, the capturing RF program is identical, but a probing bucket is turned on at a sequence of starting frequencies ranging from above the synchronous frequency in the second trace to below the synchronous frequency in the ninth trace. The energy distribution is clearly shown by the probing bucket pulses and we see that the beam was distributed throughout the area of the capturing bucket.

A quantitative check of formula (38) was attempted with the capturing voltage turned on in 7 μs as in Fig. 12, at a frequency of 71.62 Mc/s. The energy of the initial beam was below the synchronous energy and was adjusted so that the ratio of beam in the accelerated and unaccelerated peaks (trace 4, Fig. 13) is 1 to 3. The beam should then be centered on the point $-y_a$ given by formula (38), so that half is captured and half remains outside the bucket. Of the captured one-half, one-fourth is left at $+y_a$ when the voltage is turned off (accelerated peak), and one-fourth is returned to $-y_a$, leaving three-fourths of the beam unaccelerated. Table V shows the results. The frequencies of the various peaks can be accurately measured with the probing oscillator, and the corresponding energy differences calculated from the measured value of $df/dE = 45$ kc/skeV obtained as explained earlier. The resulting value of $2\Delta E$ was measured to be 14.2 keV; the calculated value for $2\,y_a = 8/\pi$ is 14.7 keV, in excellent agreement. We show also in Table V the measured frequency of the unaccelerated beam when the accelerated peak first appears. The frequency difference of 0.03 Mc/s between this and the 1 to 3 point corresponds to an energy difference of about 0.7 keV, and should correspond to half the energy spread of the beam. The two peaks become equal when the beam is at 10.5 keV (or less) from the

TABLE V

$\frac{\text{Intensity accelerated peak}}{\text{Intensity unaccelerated peak}}$	1	1/3	1/10
Frequency of accelerated peak	71.81 Mc/s	71.86 Mc/s	
Frequency of unaccelerated peak	71.36	71.25	71.22 Mc/s
Mean frequency	71.58	71.55	
Frequency difference between peaks	0.45	0.61	
Energy difference between peaks	10.5 keV	14.2 keV	

synchronous energy, showing that all of the beam is captured into a ring inside the bucket in this case. The difference 14.2 keV − 10.5 keV = 3.7 keV is again a rough measure of the energy spread in the beam, about $2\frac{1}{2}$ times larger than that obtained above. This discrepancy is easily accounted for in view of the latitude in judgement in locating the three cases to be measured. The precision of the measurements may perhaps be judged by the agreement of the two mean frequencies with the capturing radio-frequency, although even this discrepancy can be partially accounted for if the beam width is as large as 3.7 keV, by considering more carefully the way in which the pulses are placed relative to the points $\pm y_a$.

An experiment with more rapid turn-on was carried out in which the maximum and minimum energies (above and below synchronism) at which some beam is just captured were measured. The results are given in Table VI for two values of the rise time. The adiabatic value of $2\Delta E$ is calculated for $y_0 = \pm y_a$, and the sudden value for $y_0 = \pm 2$. In agreement with the digital computer result, we see that for a rise time of about $\frac{1}{2}\tau_\phi$, beam is captured between the adiabatic limits, whereas for $\tau \simeq \frac{1}{4}\tau_\phi$ beam is captured out to $y_0 = \pm 2$. (The slight difference in df/dE in Table VI as compared with the experiment of Table V is due to slight changes in the accelerator parameters between the two experiments; df/dE is measured during each experiment.) A measurement of the increase in beam energy spread was also made with the beam at the synchronous energy. For the 0.9 μs rise, the beam width increased from 3.1 keV before RF voltage is applied to 15.5 keV afterwards showing that the beam had filled the bucket. For the 2.5 μs rise, the beam width increased from 6.0 keV to 11 keV. With rise times in excess of about 4 μs, no increase in beam width was observed. These results are in general agreement with Fig. 10.

TABLE VI

RF capture experiment with fast voltage rise

Linear voltage rise time	0.9 μs	2.5 μs
Frequency of beam first captured		
E_1 (above E_s)	72.07 Mc/s	71.92 Mc/s
E_2 (below E_s)	71.03	71.23
Corresponding energy difference		
$E_1 - E_s$	10 keV	6.7 keV
$E_s - E_2$	13	8.6
$E_1 - E_2$	23	15.3
Calculated value of $2\Delta E$		
adiabatic	14.4 keV	
sudden	22.6	
df/dE	45 kc/skeV	
Period of phase oscillations	4 μs	

Acknowledgements

We wish to thank G. Ediet, D. Ford and D. Wilkinson for help in the design and construction of the RF circuitry, F. Snyder, C. Foyce and F. Anderson who developed the digital computer programs, and C. Lilliequist who carried out the digital computations on beam capture.

LIST OF REFERENCES

1. Symon, K. R. and Sessler, A. M. Methods of radio-frequency acceleration in fixed field accelerators with applications to high current and intersecting beam accelerators. CERN Symp. 1956. *1*, p. 44-58.
2. Cole, F. T., Haxby, R. O., Jones, L. W., Pruett, C. H. and Terwilliger, K. M. Electron model fixed field alternating gradient accelerator. Rev. sci. Instrum., *28*, p. 403-20, 1957.
3. Terwilliger, K. M., Jones, L. W. and Pruett, C. H. Beam stacking experiments in an electron model FFAG accelerator. Rev. sci. Instrum., *28*, p. 987-97, 1957.
4. Jones, L. W. and Terwilliger, K. M. A small model fixed field alternating gradient radial sector accelerator. CERN Symp. 1956. *1*, p. 359-65.
5. Lilliequist, C. G. and Symon, K. R. Deviations from adiabatic behavior during capture of particles into an RF bucket. MURA (*) 491. July 20, 1959.
6. Stump, R. (Private communication, to appear as a MURA (*) report.)
7. Nielsen, C. E., Symon, K.R. and Sessler, A. M. Longitudinal instabilities in intense relativistic beams. See page 239.

(*) See note on reports, p. 696.